Tunable Plasmonic Nanohole Arrays Actuated by a Thermoresponsive Hydrogel Cushion

Nityanand Sharma,[†,‡] Hamid Keshmiri,[†] Xiaodong Zhou,[∥] Ten It Wong,[∥] Christian Petri,[†,§] Ulrich Jonas,[§] Bo Liedberg,[‡] and Jakub Dostalek*,[†]

[†]Biosensor Technologies, AIT-Austrian Institute of Technology, Muthgasse 11, Wien, Austria

[‡]Centre for Biomimetic Sensor Science, School of Materials Science and Engineering, Nanyang Technological University, 50 Nanyang Drive, Singapore 637553, Singapore

[§]Macromolecular Chemistry, Department Chemistry-Biology, University of Siegen, Adolf-Reichwein-Strasse 2, Siegen 57076, Germany

[∥]Institute of Materials Research & Engineering, A*STAR, Singapore, 2 Fusionopolis Way, #08-03, Innovis, Singapore 138634, Singapore

S *Supporting Information*

ABSTRACT: New plasmonic structure with actively tunable optical characteristics based on thermoresponsive hydrogel is reported. It consists of a thin, template-stripped Au film with arrays of nanoholes that is tethered to a transparent support by a cross-linked poly(*N*-isopropylacrylamide) (pNIPAAm)-based polymer network. Upon a contact of the porous Au surface with an aqueous environment, a rapid flow of water through the pores enables swelling and collapsing of the underlying pNIPAAm network. The swelling and collapsing could be triggered by small temperature changes around the lower critical solution temperature (LCST) of the hydrogel. The process is reversible, and it is associated with strong refractive index changes of $\Delta n \sim 0.1$, which characteristically alters the spectrum of surface plasmon modes supported by the porous Au film. This approach can offer new attractive means for optical biosensors with flow-through architecture and actively tunable plasmonic transmission optical filters.
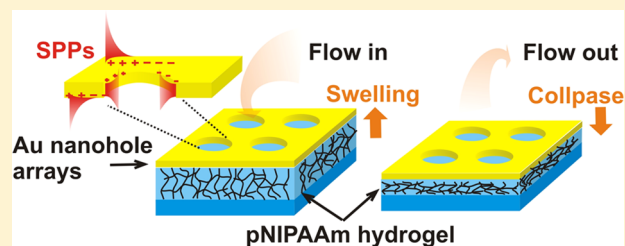
INTRODUCTION

The extraordinary transmission of light through thin metallic films with periodic nanohole arrays (NHAs)[1] has attracted substantial attention in the past decade. This phenomenon is attributed to the diffractive excitation of surface plasmon polaritons (SPPs), and it enables efficient tunneling of light through (otherwise opaque) metallic film in narrow wavelength regimes.[2,3] The transmission characteristics of metallic NHAs can be controlled by shape, depth, and periodicity of the nanoholes as well as by the type of metal and refractive index of the surrounding medium.[4−6] Plasmonic NHAs have been prepared by a range of modern fabrication techniques such as focused ion beam milling,[7] laser interference lithography,[8] electron beam lithography,[9] and template stripping.[10] The relative simplicity of design and fabrication of plasmonic NHAs have paved the way for their applications in detection and observation of biomolecules by using direct refractometric format,[7,9,11] fluorescence spectroscopy,[12] surface-enhanced Raman spectroscopy,[13] and surface-enhanced infrared absorption spectroscopy[14] as well for spectral filtering[15] and transparent electrode.[16] Conventional designs of plasmonic nanostructures are static, and their optical properties are fixed once they are prepared. In order to actuate resonant coupling to surface plasmons, metallic nanostructures have been

interfaced with inorganic materials with electro-optically[17,18] or magneto-optically[19,20] modulated refractive index. In parallel, organic materials have been explored for actuating of surface plasmon resonance by refractive index variations associated with the photochromic effects[21] and liquid crystal phase transitions[22] as well as by mechanical changes induced by specific molecular binding[23] and by responsive polymers.[24] Among the systems that utilize responsive polymers, poly(*N*-isopropylacrylamide) (pNIPAAm) based polymers (in particular copolymers with carboxylic acid groups) hold a prominent position due to their strong volumetric change upon swelling and collapsing by variation of the temperature around its lower critical solution temperature (LCST) of ~32 °C. This polymer was explored in form of brushes that surrounded[25] or directly capped[26,27] metallic nanoparticles in order to reversibly tune localized surface plasmon resonance. In addition, pNIPAAm microgels[28] were coupled with Au nanoparticles. Moreover, pNIPAAm-based networks were used as a host for Au nanoparticles[29] that displayed tunable localized surface plasmon resonance wavelength originating from near field plasmonic
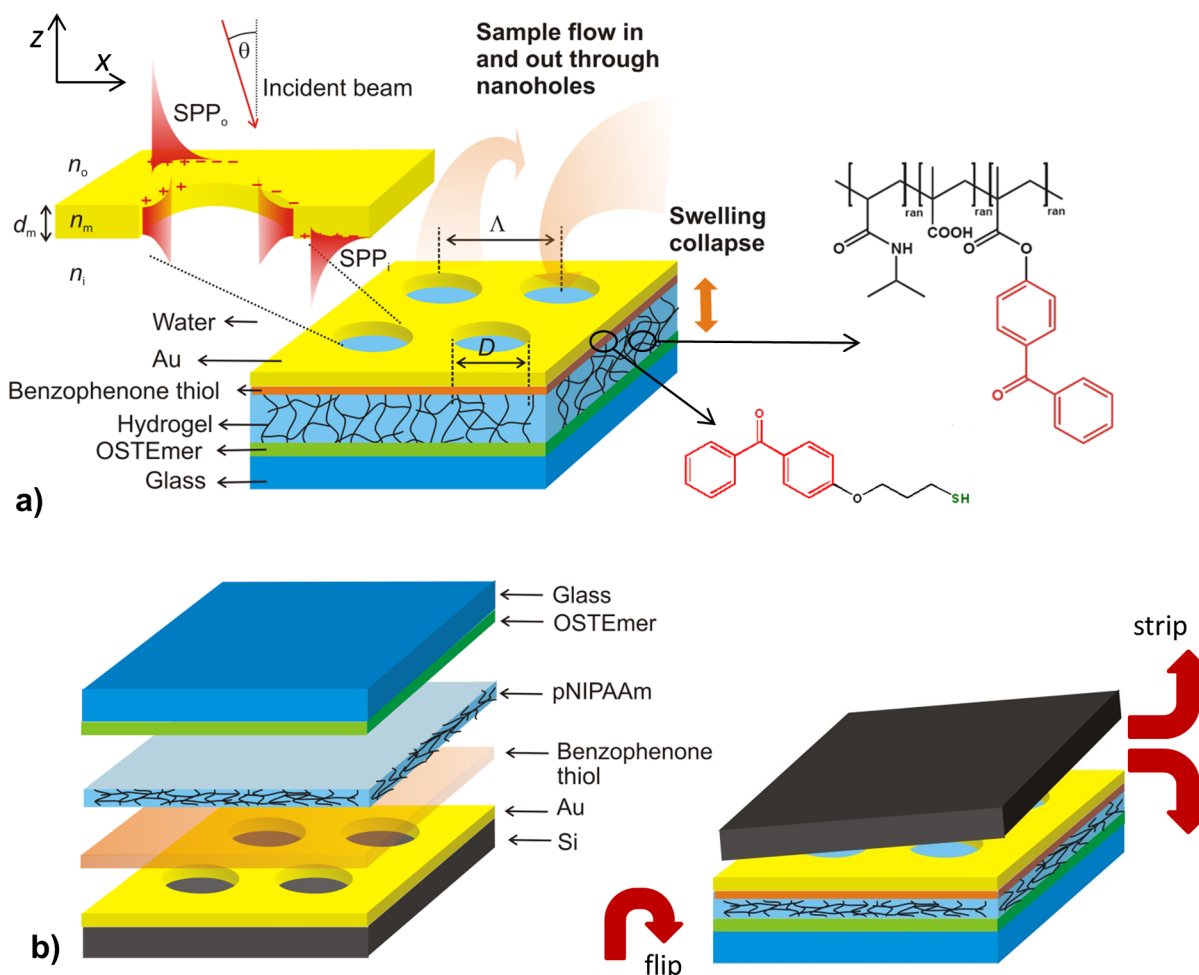
Figure 1. (a) Schematics of the investigated structure that comprise Au film with NHA that is attached to a glass substrate by a responsive pNIPAAm-based hydrogel cushion. (b) Preparation procedure of the structure by using template stripping from a Si wafer.

coupling. The swelling and collapsing of pNIPAAm-based architectures is driven by water diffusion, and the response in the millisecond range was measured for about micrometer thick cross-linked pNIPAAm-based hydrogel layer by long-range surface plasmons on the top of a indium tin oxide microheater.[30] pNIPAAm brush with a thickness of 30 nm was characterized to respond faster in about 150 μs, when rapid plasmonic heating was employed.[31] This work presents a new plasmonic structure that is tunable by thermoresponsive pNIPAAm-based hydrogel and that can be prepared by template stripping. It consists of a thin Au film with NHA that allows for diffractive coupling to propagating SPPs. This structure is tethered to a solid surface by a cross-linked pNIPAAm-based hydrogel cushion which responds to temperature variations. It can rapidly swell and collapse, which triggers a flow of water through the plasmonic pores, and it strongly modulates the refractive index by altereing the polymer fraction in the hydrogel film, leading to changes in the transmission spectrum mediated by surface plasmon modes.

METHODS

Materials. Off-stoichiometry thiol−ene polymer (OSTEmer 321) was purchased from Mercene Laboratories (Sweden). Ethanol of analysis grade was purchased from Merck Millipore (Austria). Ethylene glycol was purchased from Sigma-Aldrich (Austria). Polydimethylsiloxane (PDMS, Sylgard 184) was

purchased from Dow Corning (USA). pNIPAAm-based terpolymer (composed of N-isoproprylacrylamide, methacrylic acid, and 4-methacryloyloxybenzophenone in a ratio of 94:5:1) was synthesized as reported before.[32] (3-Thiopropyl)oxy-benzophenone (benzophenone-thiol) was synthesized as described in the literature.[33]

Preparation of Au NHA. The electron beam lithography system ELS-7000 from Elionix (Japan) was used to structure NEB22 resist layer with a thickness of 220 nm on a 600 μm thick silicon wafer with native oxide. The exposure dose of 178 μC cm^{-2} and a current of 800 pA were used and the resist was developed by o-xylene. Then, Au layer was deposited by vacuum evaporation with Denton Explorer E-beam (USA) at deposition rate of 2 Å s^{-1}. Finally, the lift-off process was accomplished by removing the NEB22 resist by soaking the wafer in remover 1165. The wafer was structured by a series of pads carrying A NHA, each with an area of 1.2 × 1.2 mm^2.

Responsive Polymer Deposition. The silicon wafer with Au NHA was incubated in an ethanolic 1 mM benzophenone-thiol solution for 24 h in order to form a self-assembled monolayer. Afterward, the surface was rinsed with ethanol and dried in a stream of air. Thin pNIPAAm layer was prepared by spin-coating an ethanolic pNIPAAm solution with a polymer concentration of 3 wt % and a spin rate of 2000 rpm for 2 min. Subsequently, the polymer layer was dried in a vacuum oven (VT6025, Thermo Scientific) overnight at T = 50 °C.

pNIPAAm-based polymer was simultaneously cross-linked and attached to Au surface by using a UV light at λ = 365 nm with an irradiation dose of 25 J cm^{-2} (UV-lamp Bio-Link 365 from Vilber, Germany). The cross-linked polymer network was rinsed thoroughly with water to remove loosely bound pNIPAAm polymer chains, and it was finally dried with a stream of air.

Template Stripping. A drop of OSTEmer 321 epoxy was placed onto the surface of a BK7 glass substrate and contacted with a flat block of PDMS in order to spread homogeneously. Then the OSTEmer 321 polymer was precured by UV light at λ = 365 nm (irradiation dose of 3 J cm^{-2}) through the PDMS block. Afterward, the PDMS block was peeled off, yielding the glass substrate with the rubbery OSTEmer layer on its top. The OSTEmer surface was pressed against the pNIPAAm film covering Au NHA on the top of a silicon wafer. In order to establish a bond between pNIPAAm and OESTEmer, the structure was kept overnight at temperature of T = 50 °C. The silicon wafer was then stripped off using a sharp blade leaving the Au NHA bonded to the glass substrate via the pNIPAAm-based layer.

Imaging of the Stripped Au NHA. Au NHA structures were characterized by scanning electron microscope (SEM) EVO from Carl Zeiss (Germany) that was operated at a low voltage of 5 kV. Atomic force microscope (AFM) Pico Plus from Molecular Imaging (USA) was used in tapping mode to observe the morphology of the dry structure. In addition, substrates with the NHA in contact with air and water were analyzed by optical microscope (BX51 M with camera SC30 from Olympus Soft Imaging Solution, Germany).

Optical Measurement. Transmission spectra were measured using an in-house developed spectroscopy system. White light emitted from a halogen lamp LSH102 from LOT-Oriel (Germany) was coupled to a multimode optical fiber M26L02 from Thorlabs (UK) and focused by an achromatic lens (f = 6 cm, 14 KLA 001 from CVI Melles Griot, Germany) at the investigated structure. The focused light beam passed through the substrate under angles between θ = 0 and 4°. The investigated structure was clamped to a transparent flow cell in order to flow aqueous samples over its surface. Temperature-dependent measurements were performed by using a Peltier device that was integrated to the flow cell. A translation stage was used to select illuminated area that carried either Au NHA or a flat Au layer as reference. Transmitted light was coupled via a lens (F810SMA-635 from Thorlabs, UK) into a multimode optical fiber (M26L02 from Thorlabs, UK) that was connected to a high-resolution spectrometer (SR-303i-B from Andor, UK). The acquired wavelength spectra were compensated for dark current. The spectra measured on the Au NHA were normalized with that obtained on a reference flat Au surface.

Simulations. The finite difference time domain (FDTD) model implemented by Lumerical Inc. (Canada) was used for simulations of the near field and far field optical properties of the investigated structure. A unit cell with the width equal to the period Λ was used and periodic Bloch boundary condition in x- and y-axes was applied (Cartesian coordinates defined in Figure 1a). In the z direction, a perfectly matched layer was placed at the distances of 1 μm above and below the layer stack. A transmission monitor was placed 0.7 μm below the Au layer. A 2D monitor in the xz-plane was employed for simulating near field distribution of the electric field intensity. The wavelength-dependent refractive index of Au n_m was obtained from the literature.[34]

■ RESULTS AND DISCUSSION

Preparation of Template Stripped NHA with Responsive PNIPAAm Cushion. As illustrated in Figure 1a, the investigated plasmonic structure consists of an Au film with rectangular NHA that is attached to a pNIPAAm-based hydrogel layer. When brought in contact with an aqueous environment, water flows thought the pores in the Au membrane into the underneath hydrogel which swells. The pNIPAAm polymer exhibits thermoresponsive properties that cause the polymer network to collapse when the structure is heated above the LCST expelling water through the porous Au membrane. The Au NHA structure with a thickness of d_m = 50 ± 1 nm was prepared on a silicon wafer with native oxide by using electron beam lithography. In order to covalently attach the pNIPAAm-based hydrogel film to the Au NHA surface, it was first modified by a self-assembled monolayer of a thiol functionalized with benzophenone groups that served as a linker for attachment of pNIPAAm-based polymer. The modified Au surface was subsequently coated by a film of the pNIPAAm-based terpolymer that carries benzophenone groups as photo-cross-linking units, as well as carboxylic acid substituents for improved swelling and for subsequent chemical modification (e.g., with biological ligands). After the pNIPAAm polymer layer was dried, it was exposed to UV in order to cross-link the polymer chains and simultaneously attach them to the Au surface by exploiting the photoreactivity of the benzophenone moieties. Afterward, the Au NHA with the pNIPAAm network layer was bonded to a UV-precured OSTEmer layer on a glass substrate (see Figure 1b). This rubbery film was pressed against the surface of the pNIPAAm film and attached via the reactive epoxy groups at elevated temperature. Finally, the stack of layers was stripped from the Si wafer to yield the surface of the Au NHA film on the top of a cross-linked pNIPAAm-based hydrogel cushion.

As seen in Figure 2a, the developed process allowed successful stripping of the Au NHA film with an underlying hydrogel layer. SEM revealed that the arrays of nanoholes retained their initial dimensions before stripping with a hole diameter of D = 208 ± 8 nm and a period of Λ = 406 ± 13 nm. Optical microscopy was used to image a corner of rectangular structured pad, as depicted in Figure 2b. The dark area in this image represents the NHA structure, and the brighter, more reflective region corresponds to the flat Au surface. Figure 2c shows an optical microscope image of the structured area that was brought in contact with water at a temperature of T = 22 °C. It indicates that the Au layer wrinkles due to the swelling of the underneath pNIPAAm hydrogel film. Such wrinkling was observed for other hydrogel films, and it is associated with stress-induced buckling, as the polymer is confined in the plane of the substrate, and thus swelling is predominantly permitted only in the direction perpendicular to the surface.[35] Afterward, the surface was dried and water rapidly diffused through the NHA pores out of the hydrogel film. Interestingly, the about 50 nm thick Au film did not exhibit cracks and defects after the swelling and drying cycle as seen in Figure 2d, acquired by optical microscopy. In addition, AFM was used for the characterization of Au NHA on the top of the hydrogel cushion after it was swollen and subsequently dried. The acquired image in Figure 2e shows that most of the pores in the Au film were filled with the pNIPAAm-based polymer network, which partially protrudes above the Au surface (visible by the brighter color of the pores in height mode). In addition, one
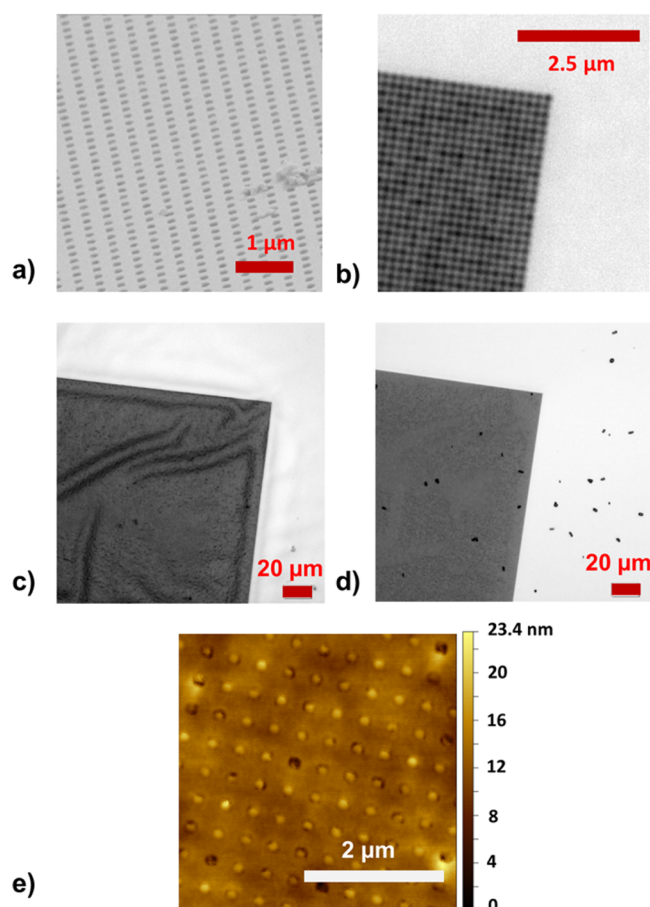
Figure 2. Observation of the stripped surface of the Au NHA by using (a) SEM and (b) optical microscopy with 100-fold magnification. (c) Optical microscopy images of an Au NHA surface with a structured pad (dark area) when swollen in water and (d) subsequently dried. (e) AFM observation of the stripped Au surface with NHAs after exposure to water followed by drying.

can see that the Au surface between the pores was smooth (root-mean-square roughness of 0.5 nm) and without cracks. It is worth mentioning that the observed low roughness at the upper interface is comparable to that of Si wafer as observed for other template stripped gold surfaces.[36] At a larger scale the Au surface became slightly undulated after swelling and collapsing of the pNIPAAm-based hydrogel, which is probably associated with the buckling and rearrangement of pNIPAAm polymer chains below the Au membrane after swelling and drying. Nevertheless, this large-scale undulation did not affect the regularity and integrity of the nanoscale dimensions of the individual pores.

Swelling Characteristics of Plain PNIPAAm Layer. Optical waveguide spectroscopy was used to characterize thickness and swelling of the pNIPAAm polymer film (analysis of measured data presented in the Supporting Information). These measurements were performed for a pNIPAAm layer that was prepared by using identical protocol on a flat Au surface. This thickness of a dry film in contact with air was measured as 212 nm, and its refractive index was $n_i = 1.48$. When the film is brought in contact with water at $T = 22$ °C, the volume fraction of the polymer chains in the hydrogel network is reduced by its swelling. Therefore, the corresponding refractive index of the pNIPAAm layer decreased to $n_i = 1.36$ (which is close to that of water [$n_0 = 1.33$] at the used

wavelength of $\lambda = 633$ nm), and the thickness increased to about 1.2 μm. At a temperature of $T = 40$ °C, hydrogel film collapsed, and its refractive index decreased to $n_i = 1.46$, which is about 0.1 refractive index units (RIU) higher than that determined in its highly swollen state at $T = 22$ °C. It should be noted that the thickness of the swollen and collapsed pNIPAAm hydrogel layer is much higher than the penetration depth of SPP field on a gold surface at wavelengths in the visible and near-infrared parts of spectrum.

Actuating Spectrum of the Surface Plasmons Modes. As indicated in Figure 1a, the thin Au film on the top of pNIPAAm layer supports SPP modes at its both interfaces. The mode that travels at the outer interface (in contact with air or with aqueous solution with refractive index n_0) is referred to as SPP_o. The mode supported by the opposite interface (in contact with pNIPAAm polymer with a refractive index n_i) is named SPP_i. The periodic NHA on the Au film allows for diffractive coupling of light into the SPP_o and SPP_i via $(\pm 1, 0)$, $(0, \pm 1)$ and higher orders. As presented in Figure 3, this coupling manifests itself as distinct resonant features in the transmission spectra. These spectra were measured with a polychromatic light beam that was focused onto the NHA, and the transmitted beam was analyzed by a spectrometer. Obtained spectra were normalized by those measured on a reference pad with a flat, nonporous 50 nm thick Au film. Two Fano resonances can be observed for the structure in contact with air in Figure 3a. They appear as a spectral band where the transmission decreases at lower wavelengths and increases at higher wavelengths. The resonance associated with the excitation of SPP_o mode at the outer interface (between Au and air) exhibits a minimum at $\lambda_o < 550$ nm (this resonance is spectrally broad as the wavelengths are close to the plasma frequency of Au). The second resonance due to the excitation of the SPP_i mode at the inner interface (between Au and dry pNIPAAm) is manifested as minimum reflectivity at around $\lambda_i = 720$ nm. As the same figure shows, the SPP_i resonance blue-shifts after the structure is brought in contact with water at a temperature of $T = 22$ °C. The SPP_i resonance wavelength λ_i is decreased by about 15 nm, which can be attributed to the swelling of pNIPAAm cushion by water diffusing through the nanoholes, accompanied by a decrease in its refractive index from n_i. The minimum of the SPP_o resonance at λ_o red-shifts by about 50 nm as the refractive index of the medium above the Au NHA structure changes from $n_0 = 1$ (air) to 1.33 (water).

The controlled permeability of the Au membrane with NHAs was tested by a series of refractometric experiments where the upper and bottom interfaces were optically probed by resonantly excited SPP_o and SPP_i modes, respectively. Aqueous samples with water spiked by ethylene glycol at concentrations between 0 and 40 vol % were used in order to change the refractive index of the outer medium between $n_0 = 1.33$ and 1.37. Transmission spectra for gradually increasing n_0 due to the ethylene glycol were measured for the swollen pNIPAAm cushion at a temperature of $T = 22$ °C. As presented in Figure 3b, both SPP_o and SPP_i resonances shift to longer wavelengths when increasing the concentration of ethylene glycol. The SPP_o resonance shifts by $\Delta\lambda_o = 9.7$ nm with the increase of ethylene glycol concentration to 40 vol %. This change corresponds to the refractive index change of $\Delta n_0 = 0.04$ RIU which yields the refractive index sensitivity of SPP_o mode of $S = \Delta\lambda_o/\Delta n_0 = 242$ nm RIU^{-1}. This value is identical to the gold grating-based SPR ($\sim$250 nm RIU^{-1} for the first order coupling at a wavelength of 600 nm),[37] and it is comparable to values typically observed on
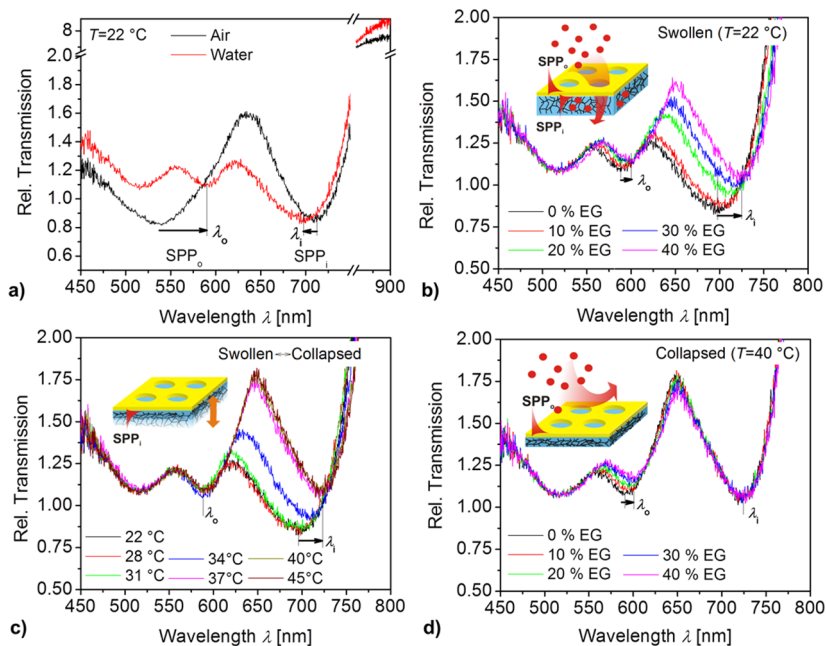
Figure 3. Measured transmission spectra for the Au NHA on top of a responsive pNIPAAm hydrogel cushion (Au NHA-hydrogel) (a) in contact with air and water at $T = 22$ °C. (b) The swollen hydrogel cushion in contact with water spiked with ethylene glycol (EG, $n_0 = 1.33-1.37$) at $T = 22$ °C. (c) Au NHA-hydrogel in water ($n_0 = 1.33$) with temperature varied in the range of $T = 22-45$ °C in order to actuate the pNIPAAm cushion. (d) The collapsed cushion in contact with water spiked with ethylene glycol ($n_0 = 1.33-1.37$) at $T = 40$ °C.
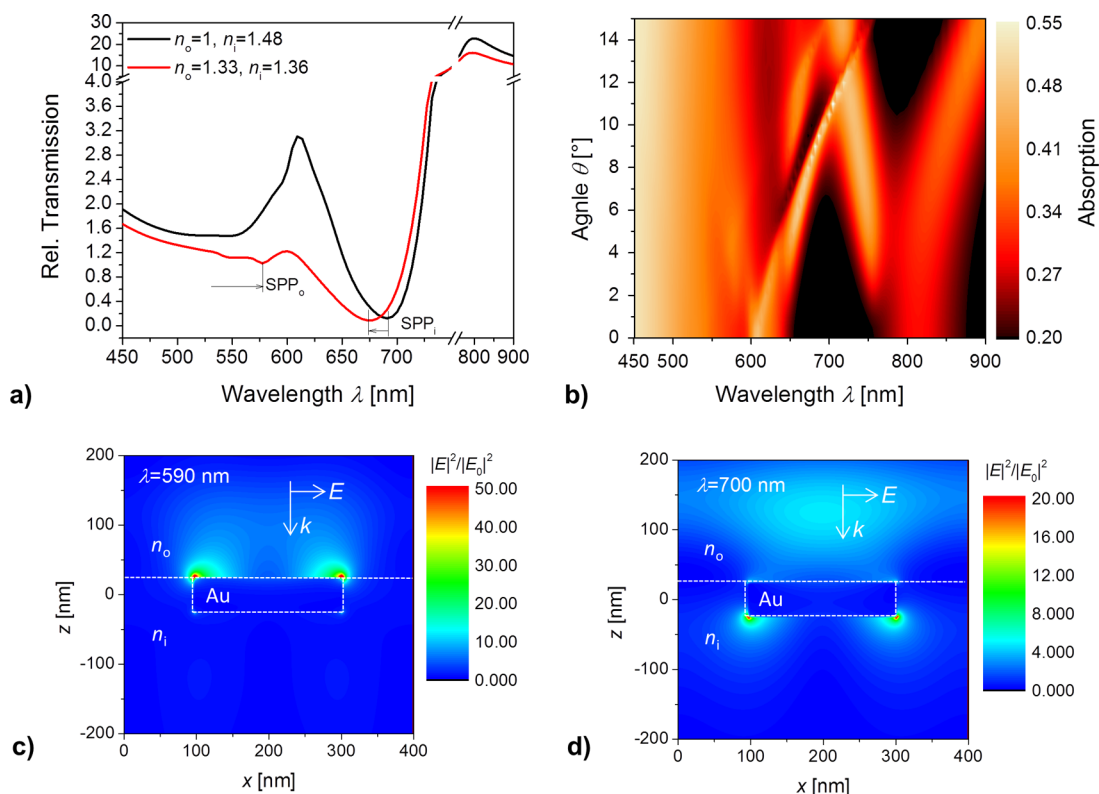

Figure 4. Simulated transmission spectra for an Au NHA-hydrogel geometry that is (a) in contact with air ($n_0 = 1$) and a collapsed hydrogel-like medium ($n_i = 1.48$) as well as with water ($n_0 = 1.33$) and a swollen hydrogel-like medium ($n_i = 1.36$), with the optical beam normal to the surface $\theta = 0°$. (b) Dispersion relation of excited SPP_i and SPP_o modes represented as absorption dependence on angle of incidence θ and wavelength λ ($n_0 = 1.33$, $n_i = 1.45$). Simulation of the near field distribution of the electric field intensity $|E/E_0|^2$ being normalized with that of the incident plane wave for a collapsed Au NHA-hydrogel structure ($n_0 = 1.33$, $n_i = 1.45$) at (c) wavelength of $\lambda = 590$ nm where the SPP_o is excited and at (d) $\lambda = 700$ nm where the SPP_i occurs.
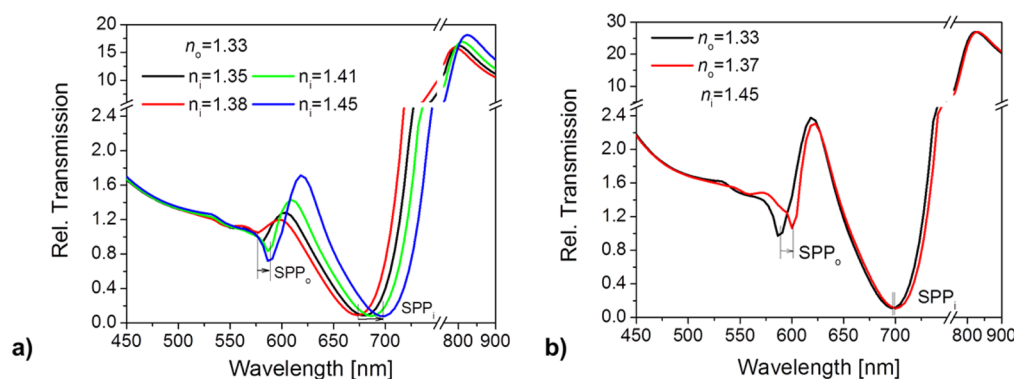
Figure 5. (a) Transmission spectra of an Au NHA-hydrogel architecture simulated for increasing refractive index n_i from 1.35 to 1.45 at the Au–hydrogel interface, representing the collapse of pNIPAAm cushion, and for an aqueous medium at the outer interface (n_0 = 1.33). (b) Transmission spectra for increasing refractive indices n_0 from 1.33 to 1.37 of the liquid medium (representative of the varying water/ethylene glycol mixtures) above the Au NHA–hydrogel film with a collapsed pNIPAAm cushion (n_i = 1.45) beneath.

Au NHA (400 nm RIU^{-1} at wavelength of 650 nm).[11] The SPP$_i$ resonance responds to ethylene glycol stronger, and it shifts by $\Delta\lambda_i$ = 26.5 nm for the maximum concentration of 40 vol %. This observation indicates that the ethylene glycol can diffuse through the NHA into the underneath swollen hydrogel. The fact that $\Delta\lambda_i$ is almost 3 times higher than $\Delta\lambda_0$ is probably due to a partial collapse of pNIPAAm triggered by ethylene glycol that provides an additional change in Δn_i.

In order to prove the identity of transmission features that were assumed to be associated with the excitation of SPP$_i$ and SPP$_o$, the refractive index was individually changed at the inner and outer side of the Au NHA structure. First, the refractive index change Δn_i was induced by the collapse of pNIPAAm cushion that is probed by SPP$_i$. In order to do so, the temperature of the water flowing over the NHA structure was gradually raised from T = 22 to 40 °C. Figure 3c reveals that the SPP$_o$ resonance (that probes the outer water medium) shifts weakly with temperature. The measured maximum shift of $\Delta\lambda_0$ = 2.5 nm can be attributed to the effect of collapsing hydrogel that partially protrudes through the nanoholes in Au film. An order of magnitude stronger shift of $\Delta\lambda_i$ = 24.5 nm was observed for the SPP$_i$ resonance due to an outward flux of water through the NHA pores and a subsequent collapse of the underlying hydrogel. The dependence of λ_i on temperature presented in the Supporting Information (Figure S2) confirms that the collapse of the pNIPAAm cushion occurs at the LSCT of 31 °C similar to the plain pNIPAAm film in direct contact with an aqueous medium without the metallic structure on top.[38] Assuming that the refractive index sensitivity of the SPP$_i$ resonance is similar to that of SPP$_o$, the measured spectral shift can be converted to refractive index change due to the pNIPAAm cushion collapse of $\Delta n_i = \Delta\lambda_i/S \sim 0.1$. Interestingly, this value is identical to that measured for swelling of pNIPAAm film without Au NHA on the top (see Figure S1).

Second, the structure was probed by SPP$_o$ and SPP$_i$ modes when refractive index at the upper interface n_0 was varied. It was utilized by collapsing pNIPAAm cushion at T = 40 °C and repeating the experiment with the flow of aqueous samples spiked with ethylene glycol over the structure. The measured data in Figure 3d indicate that the SPP$_o$ resonance responds similar as at T = 22 °C (see Figure 3b). A strong resonant wavelength shift of $\Delta\lambda_0$ = 7.5 nm was measured due to the increase in refractive index by ethylene glycol concentration of 40 vol %. This value is slightly lower than that measured for swollen pNIPAAm cushion which can be ascribed to the

collapsed polymer in the pore which partially occupies space probed in SPP$_o$ mode. The SPP$_i$ resonance shifted much weaker by only by $\Delta\lambda_i$ = 1.8 nm. This observation confirms that the hydrogel in its collapsed state prevents diffusion of molecules through the Au pores to the underneath interface that is probed by SPP$_i$.

Simulations of NHA Optical Response. The experimental data were verified by simulating transmission spectrum for the investigated Au NHA-hydrogel geometry. In these simulations the Au film was sandwiched between two semi-infinite dielectrics with refractive index n_0 and n_i. The pores were assumed to exhibit refractive index of n_i. The transmission spectra presented in Figure 4a for the dry (n_i = 1.48 and n_0 = 1) and swollen (n_i = 1.36 and n_0 = 1.33) geometry qualitatively agree with those measured at T = 22 °C (compare with Figure 3a). For the dry structure, simulations predict the SPP$_o$ resonance occurs at λ_o < 550 nm and the one associated with the SPP$_i$ mode at around λ_o = 690 nm. For the swollen structure, SPP$_o$ resonance red-shifts to around λ_o = 570 nm and the one associated with the SPP$_i$ mode blue-shifts to λ_o = 674 nm. It is worth of noting that the refractive index swollen hydrogel is similar to water which leads to the coupling of the surface plasmons across the Au layer. For such refractive index symmetrical configuration SPP$_o$ mode at lower wavelengths behaves like long-range surface plasmon for which the electric field is weakly confined in the Au layer. The SPP$_i$ mode, on the other hand, behaves like a short-range surface plasmon with the corresponding electric field strongly confined in the Au film. When the hydrogel film is collapsed (n_0 = 1.33 and n_i = 1.46), the symmetry is broken and individual SPP$_i$ and SPP$_o$ modes propagate along individual interfaces. Figure 4b illustrates for such a geometry the dispersion relation of SPP$_i$ and SPP$_o$ modes represented as absorption dependence on the angle of incidence θ and wavelength λ. It reveals complex behavior where resonances associated with the first-order coupling to SPP$_o$ and SPP$_i$ split and cross when increasing θ. In addition, flattening of SPP bands for low angle θ occurs.

In order to check for the identity of the used resonances, the near field distribution of the electric field intensity was simulated at the wavelengths 590 and 700 nm, as seen in Figures 4c and 4d, respectively. These images confirm that the shorter wavelength resonance SPP$_o$ is probing the outer interface of the Au NHA-hydrogel film in contact with water, while the inner interface in contact with the polymer layer is probed by the longer wavelength SPP$_i$ resonance.

Finally, sensitivity of SPP_o and SPP_i resonances to the refractive index variations above and below the Au NHA was theoretically studied. The simulated transmission spectra for n_i varying between 1.35 and 1.45 and fixed $n_0 = 1.33$ are presented in Figure 5a. These data resembles the temperature-dependent experiment with collapsing the gel (presented in Figure 3c) They show a strong shift in the SPP_i resonance of $\Delta\lambda_i = 24$ nm, which is similar to the experimentally measured value. In accordance with experimental results, the simulations predict less pronounced changes in the SPP_o resonance of $\Delta\lambda_o = 11.5$ nm for refractive index change in n_i. Figure 5b describes the complementary case when the refractive index above the Au surface n_0 is varied. These simulations are related to the experiment in Figure 3d where the refractive index n_0 of the liquid medium was changed from 1.33 to 1.37 (by variation of the water/ethylene glycol mixing ratio), while the pNIPAAm hydrogel cushion with $n_i = 1.46$ was collapsed above the LCST ($T = 40$ °C). The obtained simulation results predict a shift of about $\Delta\lambda_o = 13$ nm of the SPP_o resonance wavelength. In accordance with the experimental findings, the response of SPP_i mode of $\Delta\lambda_o \sim 3$ nm is much smaller. We believe that deviation between the experiment and simulations can be mostly attributed to the protrusion of hydrogel present in the pores beyond the upper interface. This leads to additional refractive index changes that are not taken into account in the model.

CONCLUSIONS

A facile template-stripping approach to tether a thin Au NHA to a thermoresponsive hydrogel cushion is reported, and the optical properties of such structure are characterized in detail. A series of experiments show that water flow through the pores in Au NHA can be controlled by swelling the underneath hydrogel. When the hydrogel collapses upon temperature increase, water is expelled through the pores, and then they become nonpermeable/closed. In the swollen state the low polymer volume fraction in the hydrogel generates a symmetric refractive index configuration for both interfaces (Au-liquid medium and Au-hydrogel), which establishes long-range and short-range SPPs. When the gel is collapsed, the refractive index symmetry is perturbed and distinct SPPs exist at the individual interfaces. Reversible swelling and collapsing of the hydrogel is accompanied by a strong refractive index change of 0.1, which can be used for tuning the wavelength at which plasmonically enhanced transmission occurs. Because of the rapid response to the temperature variations around the LCST,[30] this approach may find its applications in actively tunable optical filters. The reported structure can also be implemented in plasmonic biosensing, where analyzed samples are flowed through the plasmonic nanoholes in order to overcome diffusion-limited mass transfer of target analyte to the surface. In current sensor setups such an architecture is typically realized by using thin nitride membranes which require multiple lithography steps.[9,39] The presented approach may provide simpler means for device preparation, and it holds potential to harness this intriguing biosensor concept in more practical devices. In conjunction with field intensity enhancement occurring at the nanohole plasmonic hotspot, the more efficient capture of target analyte at the surface offers attractive means to advance sensitivity in direct refractometric detection of biomolecules as well as in sensors relying on plasmonically amplified spectroscopy.

ASSOCIATED CONTENT

Ⓢ Supporting Information

The Supporting Information is available free of charge on the ACS Publications website at DOI: 10.1021/acs.jpcc.5b10336.

Investigation of swelling and collapsing of a pNIPAAm-based hydrogel layer by optical waveguide spectroscopy (Figure S1); evaluated changes in SPP resonant wavelengths for Au NHA on pNIPAAm hydrogel cushion (Figure S2) from curves presented in Figure 3 (PDF)

AUTHOR INFORMATION

Corresponding Author

*E-mail jakub.dostalek@ait.ac.at (J.D.).

Notes

The authors declare no competing financial interest.

REFERENCES

(1) Ebbesen, T. W.; Lezec, H. J.; Ghaemi, H. F.; Thio, T.; Wolff, P. A. Extraordinary Optical Transmission through Sub-Wavelength Hole Arrays. *Nature* **1998**, *391*, 667−669.

(2) Martín-Moreno, L.; García-Vidal, F. J.; Lezec, H. J.; Pellerin, K. M.; Thio, T.; Pendry, J. B.; Ebbesen, T. W. Theory of Extraordinary Optical Transmission through Subwavelength Hole Arrays. *Phys. Rev. Lett.* **2001**, *86*, 1114−1117.

(3) Genet, C.; Ebbesen, T. W. Light in Tiny Holes. *Nature* **2007**, *445*, 39−46.

(4) Grupp, D. E.; Lezec, H. J.; Ebbesen, T. W.; Pellerin, K. M.; Thio, T. Crucial Role of Metal Surface in Enhanced Transmission through Subwavelength Apertures. *Appl. Phys. Lett.* **2000**, *77*, 1569−1571.

(5) Koerkamp, K. J. K.; Enoch, S.; Segerink, F. B.; van Hulst, N. F.; Kuipers, L. Strong Influence of Hole Shape on Extraordinary Transmission through Periodic Arrays of Subwavelength Holes. *Phys. Rev. Lett.* **2004**, *92*, 183901.

(6) van der Molen, K. L.; Klein Koerkamp, K. J.; Enoch, S.; Segerink, F. B.; van Hulst, N. F.; Kuipers, L. Role of Shape and Localized Resonances in Extraordinary Transmission through Periodic Arrays of Subwavelength Holes: Experiment and Theory. *Phys. Rev. B: Condens. Matter Mater. Phys.* **2005**, *72*, 045421.

(7) Eftekhari, F.; Escobedo, C.; Ferreira, J.; Duan, X.; Girotto, E. M.; Brolo, A. G.; Gordon, R.; Sinton, D. Nanoholes as Nanochannels: Flow-through Plasmonic Sensing. *Anal. Chem.* **2009**, *81*, 4308−4311.

(8) Tetz, K. A.; Pang, L.; Fainman, Y. High-Resolution Surface Plasmon Resonance Sensor Based on Linewidth-Optimized Nanohole Array Transmittance. *Opt. Lett.* **2006**, *31*, 1528−1530.

(9) Yanik, A. A.; Huang, M.; Kamohara, O.; Artar, A.; Geisbert, T. W.; Connor, J. H.; Altug, H. An Optofluidic Nanoplasmonic Biosensor for Direct Detection of Live Viruses from Biological Media. *Nano Lett.* **2010**, *10*, 4962−4969.

(10) Im, H.; Lee, S. H.; Wittenberg, N. J.; Johnson, T. W.; Lindquist, N. C.; Nagpal, P.; Norris, D. J.; Oh, S. H. Template-Stripped Smooth Ag Nanohole Arrays with Silica Shells for Surface Plasmon Resonance Biosensing. *ACS Nano* **2011**, *5*, 6244−6253.

(11) Brolo, A. G.; Gordon, R.; Leathem, B.; Kavanagh, K. L. Surface Plasmon Sensor Based on the Enhanced Light Transmission through Arrays of Nanoholes in Gold Films. *Langmuir* **2004**, *20*, 4813−4815.

(12) Brolo, A. G.; Kwok, S. C.; Moffitt, M. G.; Gordon, R.; Riordon, J.; Kavanagh, K. L. Enhanced Fluorescence from Arrays of Nanoholes in a Gold Film. *J. Am. Chem. Soc.* **2005**, *127*, 14936−14941.

(13) Kumar, S.; Cherukulappurath, S.; Johnson, T. W.; Oh, S. H. Millimeter-Sized Suspended Plasmonic Nanohole Arrays for Surface-Tension-Driven Flow-through Sers. *Chem. Mater.* **2014**, *26*, 6523−6530.

(14) Coe, J. V.; Rodriguez, K. R.; Teeters-Kennedy, S.; Cilwa, K.; Heer, J.; Tian, H.; Williams, S. M. Metal Films with Arrays of Tiny Holes: Spectroscopy with Infrared Plasmonic Scaffolding. *J. Phys. Chem. C* **2007**, *111*, 17459−17472.

(15) Najiminaini, M.; Vasefi, F.; Kaminska, B.; Carson, J. J. Nanohole-Array-Based Device for 2d Snapshot Multispectral Imaging. *Sci. Rep.* **2013**, *3*, 2589.

(16) Chou, S. Y.; Ding, W. Ultrathin, High-Efficiency, Broad-Band, Omni-Acceptance, Organic Solar Cells Enhanced by Plasmonic Cavity with Subwavelength Hole Array. *Opt. Express* **2013**, *21* (Suppl. 1), A60−A76.

(17) Dicken, M. J.; Sweatlock, L. A.; Pacifici, D.; Lezec, H. J.; Bhattacharya, K.; Atwater, H. A. Electrooptic Modulation in Thin Film Barium Titanate Plasmonic Interferometers. *Nano Lett.* **2008**, *8*, 4048−4052.

(18) Rosenkrantz, E.; Arnon, S. Local Surface Plasmon Tuning for Optical Devices. *IEEE Photonics Technol. Lett.* **2015**, *27*, 669−672.

(19) Temnov, V. V.; Armelles, G.; Woggon, U.; Guzatov, D.; Cebollada, A.; Garcia-Martin, A.; Garcia-Martin, J. M.; Thomay, T.; Leitenstorfer, A.; Bratschitsch, R. Active Magneto-Plasmonics in Hybrid Metal-Ferromagnet Structures. *Nat. Photonics* **2010**, *4*, 107−111.

(20) Hermann, C.; Kosobukin, V. A.; Lampel, G.; Peretti, J.; Safarov, V. I.; Bertrand, P. Surface-Enhanced Magneto-Optics in Metallic Multilayer Films. *Phys. Rev. B: Condens. Matter Mater. Phys.* **2001**, *64*, 235422.

(21) Pala, R. A.; Shimizu, K. T.; Melosh, N. A.; Brongersma, M. L. A Nonvolatile Plasmonic Switch Employing Photochromic Molecules. *Nano Lett.* **2008**, *8*, 1506−1510.

(22) Liu, Y. J.; Si, G. Y.; Leong, E. S.; Xiang, N.; Danner, A. J.; Teng, J. H. Light-Driven Plasmonic Color Filters by Overlaying Photo-responsive Liquid Crystals on Gold Annular Aperture Arrays. *Adv. Mater.* **2012**, *24*, OP131−OP135.

(23) Piantanida, L.; Naumenko, D.; Torelli, E.; Marini, M.; Bauer, D. M.; Fruk, L.; Firrao, G.; Lazzarino, M. Plasmon Resonance Tuning Using DNA Origami Actuation. *Chem. Commun.* **2015**, *51*, 4789−4792.

(24) Chen, K.; Leong, E. S. P.; Rukavina, M.; Nagao, T.; Liu, Y. J.; Zheng, Y. Active Molecular Plasmonics: Tuning Surface Plasmon Resonances by Exploiting Molecular Dimensions. *Nanophotonics* **2015**, *4*, 186−197.

(25) Mitsuishi, M.; Koishikawa, Y.; Tanaka, H.; Sato, E.; Mikayama, T.; Matsui, J.; Miyashita, T. Nanoscale Actuation of Thermoreversible Polymer Brushes Coupled with Localized Surface Plasmon Resonance of Gold Nanoparticles. *Langmuir* **2007**, *23*, 7472−7474.

(26) Gehan, H.; Mangeney, C.; Aubard, J.; Levi, G.; Hohenau, A.; Krenn, J. R.; Lacaze, E.; Felidj, N. Design and Optical Properties of Active Polymer-Coated Plasmonic Nanostructures. *J. Phys. Chem. Lett.* **2011**, *2*, 926−931.

(27) Nguyen, M.; et al. Engineering Thermoswitchable Lithographic Hybrid Gold Nanorods as Plasmonic Devices for Sensing and Active Plasmonics Applications. *ACS Photonics* **2015**, *2*, 1199−1208.

(28) Karg, M.; Pastoriza-Santos, I.; Perez-Juste, J.; Hellweg, T.; Liz-Marzan, L. M. Nanorod-Coated Pnipam Microgels: Thermoresponsive Optical Properties. *Small* **2007**, *3*, 1222−1229.

(29) Matsui, J.; Akamatsu, K.; Hara, N.; Miyoshi, D.; Nawafune, H.; Tamaki, K.; Sugimoto, N. Spr Sensor Chip for Detection of Small Molecules Using Molecularly Imprinted Polymer with Embedded Gold Nanoparticles. *Anal. Chem.* **2005**, *77*, 4282−4285.

(30) Toma, M.; Jonas, U.; Mateescu, A.; Knoll, W.; Dostalek, J. Active Control of Spr by Thermoresponsive Hydrogels for Biosensor Applications. *J. Phys. Chem. C* **2013**, *117*, 11705−11712.

(31) Winkler, P.; Belitsch, M.; Tischler, A.; Häfele, V.; Ditlbacher, H.; Krenn, J. R.; Hohenau, A.; Nguyen, M.; Félidj, N.; Mangeney, C. Nanoplasmonic Heating and Sensing to Reveal the Dynamics of Thermoresponsive Polymer Brushes. *Appl. Phys. Lett.* **2015**, *107*, 141906.

(32) Junk, M. J.; Jonas, U.; Hinderberger, D. Epr Spectroscopy Reveals Nanoinhomogeneities in the Structure and Reactivity of Thermoresponsive Hydrogels. *Small* **2008**, *4*, 1485−1493.

(33) Anac, I.; Aulasevich, A.; Junk, M. J. N.; Jakubowicz, P.; Roskamp, R. F.; Menges, B.; Jonas, U.; Knoll, W. Optical Characterization of Co-Nonsolvency Effects in Thin Responsive Pnipaam-Based Gel Layers Exposed to Ethanol/Water Mixtures. *Macromol. Chem. Phys.* **2010**, *211*, 1018−1025.

(34) Palik, E. D. *Handbook of Optical Constants of Solids*; Academic Press: 1998.

(35) Guvendiren, M.; Yang, S.; Burdick, J. A. Swelling-Induced Surface Patterns in Hydrogels with Gradient Crosslinking Density. *Adv. Funct. Mater.* **2009**, *19*, 3038−3045.

(36) Hegner, M.; Wagner, P.; Semenza, G. Ultralarge Atomically Flat Template-Stripped Au Surfaces for Scanning Probe Microscopy. *Surf. Sci.* **1993**, *291*, 39−46.

(37) Homola, J.; Koudela, I.; Yee, S. S. Surface Plasmon Resonance Sensors Based on Diffraction Gratings and Prism Couplers: Sensitivity Comparison. *Sens. Actuators, B* **1999**, *54*, 16−24.

(38) Beines, P. W.; Klosterkamp, I.; Menges, B.; Jonas, U.; Knoll, W. Responsive Thin Hydrogel Layers from Photo-Cross-Linkable Poly-(N-Isopropylacrylamide) Terpolymers. *Langmuir* **2007**, *23*, 2231−2238.

(39) Escobedo, C.; Brolo, A. G.; Gordon, R.; Sinton, D. Optofluidic Concentration: Plasmonic Nanostructure as Concentrator and Sensor. *Nano Lett.* **2012**, *12*, 1592−1596.